Embedded Nanostructures Revealed in Three Dimensions

I. Arslan, *et al.*

Science **309**, 2195 (2005);
DOI: 10.1126/science.1116745

(blue) and negative (black) bias at different injection positions along the channel. Both the amplitude and width of the curves decrease with increasing distance from the drain contact, similar to the previous $\theta_K(B_y)$ data. These data provide conclusive evidence that the Fe/GaAs Schottky tunnel barriers in lateral devices function as both spin detectors and injectors.

These measurements provide a detailed picture of spin transport in simple ferromagnet/semiconductor lateral structures. Smaller lateral dimensions and additional components, including a means to switch the source and drain contacts independently, will enhance the functionality of these devices. Although developing a purely electrical spin-transport device using a field effect or other means for spin manipulation remains a great challenge (*29*), the integration of an electrical injector and detector in a lateral structure represents an important step toward this goal.

References and Notes

1. A. T. Hanbicki *et al.*, *Appl. Phys. Lett.* **82**, 4092 (2003).
2. X. Jiang *et al.*, *Phys. Rev. Lett.* **94**, 056601 (2005).
3. C. Adelmann, X. Lou, J. Strand, C. J. Palmstrøm, P. A. Crowell, *Phys. Rev. B* **71**, 121301 (2005).
4. V. F. Motsnyi *et al.*, *Appl. Phys. Lett.* **81**, 265 (2002).
5. J. M. Kikkawa, D. D. Awschalom, *Nature* **397**, 139 (1999).
6. Y. Kato, R. C. Myers, A. C. Gossard, D. D. Awschalom, *Nature* **427**, 50 (2004).
7. S. A. Crooker, D. L. Smith, *Phys. Rev. Lett.* **94**, 236601 (2005).
8. Y. K. Kato, R. C. Myers, A. C. Gossard, D. D. Awschalom, *Phys. Rev. Lett.* **93**, 176601 (2004).
9. Y. K. Kato, R. C. Myers, A. C. Gossard, D. D. Awschalom, *Science* **306**, 1910 (2004).
10. J. Wunderlich, B. Kaestner, J. Sinova, T. Jungwirth, *Phys. Rev. Lett.* **94**, 047204 (2005).
11. M. Johnson, R. H. Silsbee, *Phys. Rev. Lett.* **55**, 1790 (1985).
12. F. J. Jedema, H. B. Heersche, A. T. Filip, J. J. A. Baselmans, B. J. van Wees, *Nature* **416**, 713 (2002).
13. P. R. Hammar, B. R. Bennett, M. J. Yang, M. Johnson, *Phys. Rev. Lett.* **83**, 203 (1999).
14. F. G. Monzon, H. X. Tang, M. L. Roukes, *Phys. Rev. Lett.* **84**, 5022 (2000).
15. B. J. Van Wees, *Phys. Rev. Lett.* **84**, 5023 (2000).
16. P. R. Hammar, M. Johnson, *Phys. Rev. Lett.* **88**, 066806 (2002).
17. Materials and methods are available as supporting material on *Science* Online.
18. J. Stephens *et al.*, *Phys. Rev. Lett.* **93**, 097602 (2004).
19. G. E. Pikus, A. N. Titkov, in *Optical Orientation*, F. Meier, B. P. Zakharchenya, Eds. (North-Holland, Amsterdam, 1984), pp. 73–131.
20. C. Ciuti, J. P. McGuire, L. J. Sham, *Phys. Rev. Lett.* **89**, 156601 (2002).
21. R. K. Kawakami *et al.*, *Science* **294**, 131 (2001).
22. R. J. Epstein *et al.*, *Phys. Rev. B* **65**, 121202R (2002).
23. The temporal integral in Eq. 1 is the one-dimensional, strain-free, Green's-function solution to the drift-diffusion equation.
24. Y. K. Kato, R. C. Myers, A. C. Gossard, D. D. Awschalom, *Appl. Phys. Lett.* **87**, 022503 (2005).
25. Z. G. Yu, M. E. Flatte, *Phys. Rev. B* **66**, 201202R (2002).
26. The absence of a ferromagnet in the injection region of these lateral devices and the detection of transverse spin at small magnetic fields avoid complications that have affected previous efforts to electrically detect optically oriented spins (*27*, *28*).
27. A. Hirohata, Y. B. Xu, C. M. Guertler, J. A. C. Bland, S. N. Holmes, *Phys. Rev. B* **63**, 104425 (2001).
28. A. F. Isakovic *et al.*, *J. Appl. Phys.* **91**, 7261 (2002).
29. S. Datta, B. Das, *Appl. Phys. Lett.* **56**, 665 (1990).

30. We thank L. Sham for valuable discussions and H.-J. Jang for technical assistance. This work was supported by the Defense Advanced Research Projects Agency's SpinS and Los Alamos Laboratory Directed Research and Development programs, the NSF Materials Research Science and Engineering Center program under grant DMR 02-12032, the Office of Naval Research, and the Minnesota Nanofabrication Center, which is supported by the NSF National Nanotechnology Infrastructure Network program.

Supporting Online Material

www.sciencemag.org/cgi/content/full/309/5744/2191/DC1
Materials and Methods
Figs. S1 to S3

1 July 2005; accepted 25 August 2005
10.1126/science.1116865

Embedded Nanostructures Revealed in Three Dimensions

I. Arslan,[1]* T. J. V. Yates,[1] N. D. Browning,[2,3] P. A. Midgley[1]

Nanotechnology creates a new challenge for materials characterization because device properties now depend on size and shape as much as they depend on the traditional parameters of structure and composition. Here we show that Z-contrast tomography in the scanning transmission electron microscope has been developed to determine the complete three-dimensional size and shape of embedded structures with a resolution of approximately 1 cubic nanometer. The results from a tin/silicon quantum dot system show that the positions of the quantum dots and their size, shape, structure, and formation mechanism can be determined directly. These methods are applicable to any system, providing a unique and versatile three-dimensional visualization tool.

The past decade has seen device technology enter the realm of nanoscale engineering for a large number of different applications. Many applications involve nanostructures that are embedded in other materials, where it is the size, shape, composition, and chemical interaction with the matrix that are key in determining the overall functionality of the device. Site-specific quantum-dot markers in live cells (*1*), inorganic nanostructures within self-assembled organic or biological templates (*2*), semiconductor nanocrystals (*3*) and metal tips grown on quantum rods and tetrapods (*4*), and catalytic growth of nanowires and nanostructures (*5*) are just some examples of new systems where the size, shape, and location (interaction) of the nanostructures are the critical parameters.

Transmission electron microscopy (TEM) and its variants have given us insight into nanoscale materials issues for over half a century. However, the vast majority of previous studies have made use of the periodicity of the sample (crystal structure) in the direction of the beam propagation, and they only involved the recording of a single two-dimensional (2D) projection (image) to understand the relationships between the structure and its properties. In nanostructures, the periodicity of the crystal structure in the beam direction does not continue indefinitely, and in fact, exactly when and how the periodicity terminates determines the material's properties. In such a case, a single 2D projection of the 3D object can at best give only partial information, and at worst be very misleading. Overcoming the ambiguity in the interpretation of a single 2D projection has been the driving force behind the very recent development of electron tomography that allows materials to be studied in 3D.

The conventional method to study structures with TEM is through high-resolution phase-contrast imaging (*6*, *7*). However, the relatively new technique of scanning transmission electron microscopy (STEM) can be superior to conventional TEM for some materials applications because of the incoherent nature of the imaging, the sensitivity to the atomic number Z of the species in the samples (Z-contrast imaging), direct interpretability, and the possibility of concurrent spectroscopy on the atomic scale (*8*–*12*). In general, electron tomography using Z-contrast imaging in a STEM is the most useful way to study crystalline inorganic nanomaterials in 3D. The reason is that diffraction contrast, which is seen in many bright-field and dark-field TEM images, violates the projection requirement, which states that the signal used for tomographic reconstructions must be a monotonic function of a physical property (*13*). The projection requirement must be fulfilled for a successful 3D reconstruction of the object from the series of 2D tilt images.

We used STEM tomography to study tin-rich (Sn) quantum dots embedded in a silicon

[1]Department of Materials Science and Metallurgy, University of Cambridge, Pembroke Street, Cambridge, CB2 3QZ, UK. [2]Department of Chemical Engineering and Materials Science, University of California, One Shields Avenue, Davis, CA 95616, USA. [3]National Center for Electron Microscopy, Lawrence Berkeley National Laboratory, One Cyclotron Road, Berkeley, CA 94720, USA.

*To whom correspondence should be addressed. E-mail: ia250@cam.ac.uk

(Si) matrix with a resolution of ~1 nm^3. Quantum dots are important nanostructures for optoelectronic devices that exploit quantum confinement for discrete energy levels in the dot with a bandgap smaller than the matrix (*14*–*16*). For correct device functionality, the 3D size, shape, distribution, and composition of all the dots must be uniform. It has been shown that Sn_xSi_{1-x} alloy layers with $x \leq 0.1$ grown on Si (100) form α-Sn quantum dots (*17*–*19*). In order for this alloying to take place, Si atoms from the surrounding matrix must diffuse into the Sn layer. This in turn creates vacancies in the Si, which group together to form voids (*20*, *21*). These voids have been shown to have a distinct equilibrium shape, namely a truncated octahedron, or a tetrakaidecahedron (*22*). Previous 2D EM studies (*18*, *19*) have shown that the α-Sn dots also exhibit this faceted shape in the embedded layer (formed by phase separation). This is perhaps not so surprising because α-Sn and Si have the same cubic crystal structure and therefore the same equilibrium shape. However, dots of apparently the same morphology were also observed to form outside of the embedded layers, but the mechanism for such growth could not be identified. In-situ heating experiments (*18*) showed that Sn diffused out of the embedded layer and into the Si voids that were formed due to strain during the growth process (*18*, *19*), thus creating the out-of-layer quantum dots.

Electron tomography was performed on an FEI Tecnai F20 electron microscope (FEI, Eindhaven, Netherlands) at an accelerating voltage of 200 kV at the University of Cambridge. 149 Z-contrast tilt images were taken every 1° over the tilt range of –74° to +74°. The reconstructions were performed using Inspect 3D software [reconstruction techniques described in (*13*)] and visualized using Amira. Figure 1A shows a single image from the series at 0° tilt. Figure 1B shows the tomographic reconstruction of this tilt series, and by comparing the two figures, it is clear that the dots are in the same position and are the same size in projection, indicating a good reconstruction. Figure 1C is the perpendicular projection of the reconstruction, showing that this volume of material actually consists of two layers of quantum dots, with one small dot above the bottom layer, indicated by an arrow. This small dot between the layers is of particular interest because it provides evidence of how the Sn fills the Si voids. The apparently agglomerated dots seen below the layer were not studied, because they are close to the surface and may have transformed into a different phase because of their interaction with the air, or they may have been damaged from specimen preparation techniques. To enable a better view of the small dot between the layers, a second reconstruction was performed incorporating only the small volume surrounding the out-of-layer quantum dot at a far higher spatial resolution. Figure 1, D and E, shows this reconstruction in (001) plan view and (110) cross section, respectively. These panels demonstrate that there are clear facets on all the quantum dots (movie S1), and that although most of them appear to have the same equi-sized shape, there are a number that appear elongated along perpendicular crystal dimensions (see later discussion of this phenomenon).

To have a basis with which to analyze the out-of-layer dot, we first examined one that is in the layer, approximately 7 nm in diameter. Figure 2, A and B, shows the reconstruction of this quantum dot in the (100) and (110) orientations. The insets show the same image with a superimposed outline of a perfect tetrakaidecahedron in those respective orientations. It can be seen from the figures, the insets, and movie S2 that this dot is of uniform width in 3D and fits the assumed truncated octahedron shape proposed from the 2D analysis. Figure 2, C and D, shows the out-of-layer dot, approximately 3.5 nm in diameter. By looking at the projections of the reconstruction of this dot in the (100) and (110) orientations and movie S3, we can see that this dot is not as uniform as are the in-layer dots. Some of the dot is missing in the upper left corner of the overlaid structure (Fig. 2C, inset) and the dot has filled less of the right side of the overlaid structure compared with the left (Fig. 2D, inset). This evidence suggests that the voids are being filled by Sn from one side.

This type of filling is identical to that which has been observed previously for metal precipitates and voids of similar sizes (*23*, *24*).

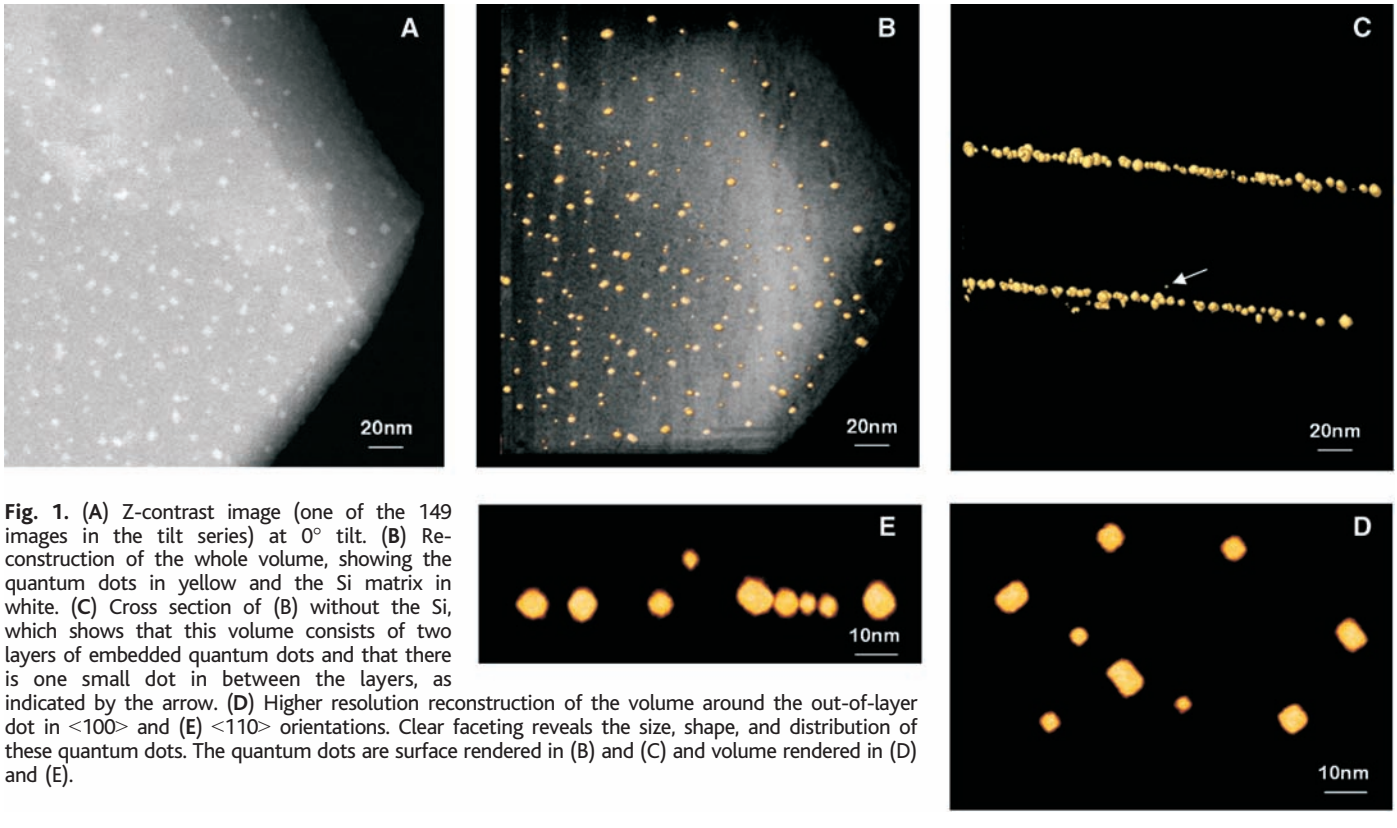

Fig. 1. (**A**) Z-contrast image (one of the 149 images in the tilt series) at 0° tilt. (**B**) Reconstruction of the whole volume, showing the quantum dots in yellow and the Si matrix in white. (**C**) Cross section of (B) without the Si, which shows that this volume consists of two layers of embedded quantum dots and that there is one small dot in between the layers, as indicated by the arrow. (**D**) Higher resolution reconstruction of the volume around the out-of-layer dot in <100> and (**E**) <110> orientations. Clear faceting reveals the size, shape, and distribution of these quantum dots. The quantum dots are surface rendered in (B) and (C) and volume rendered in (D) and (E).

Whereas the bonding in metals and semiconductors is different (metallic versus covalent), the similarities in the formation mechanism indicate that the shape and size of embedded nanostructures may be driven by the same mechanism for all systems. Rich *et. al*. (*25*) studied monolayer growth of Sn on Si (100) and found that after ~1.5 monolayers of deposition, the growth becomes 3D, forming clusters that then coalesce. From high-resolution synchrotron photoemission spectra, they were able to deduce that there are two distinct adsorption sites of Sn on Si (100), called S1 and S2. For coverages between 0 to 0.2 monolayers, the S1 sites dominate; for coverages between 0.2 to 0.68 monolayers, the S1 and S2 site populations are nearly equal; and for coverages above 1 monolayer, the S1 sites dominate again. It is believed that the S2 sites lie below the S1 sites, with the Sn atoms preferentially replacing the surface Si atoms located in a dimerized layer, whereas the S1 sites are dispersed on the surface, bonding to two Si surface atoms equivalently. The domination of these surface sites at coverages beyond 1 monolayer indicates a path for the initiation of the 3D growth observed. Similar results have been found for Sn on Si (111) with spectroscopic measurements (*26*), as well as direct scanning tunneling microscopy imaging showing the formation of 3D α-Sn islands on the Si (111) surface (*27*). Experiments have pointed to three distinct growth modes: layer-by-layer Frank–Van der Merwe growth; 3D nucleation upon contact, called Volmer-Weber growth; and Stranski-Krastonov growth, in which a few monolayers are adsorbed layer-by-layer before a transition to 3D growth (*24*). Based on our findings and those in (*24*–*27*), it appears that the system described here follows Stranski-Krastonov growth. The initial monolayer growth that wets the surface of the void is not resolved in the tomographic reconstruction, but the high-resolution Z-contrast images in (*18*) hint at this with slightly higher contrast around the edges of the quantum dot. However, the subsequent 3D growth is consistent with the observations presented here, because we see the void being filled from one side, indicating there has been 3D nucleation of the Sn inside the void that would then propagate until it reaches the other side.

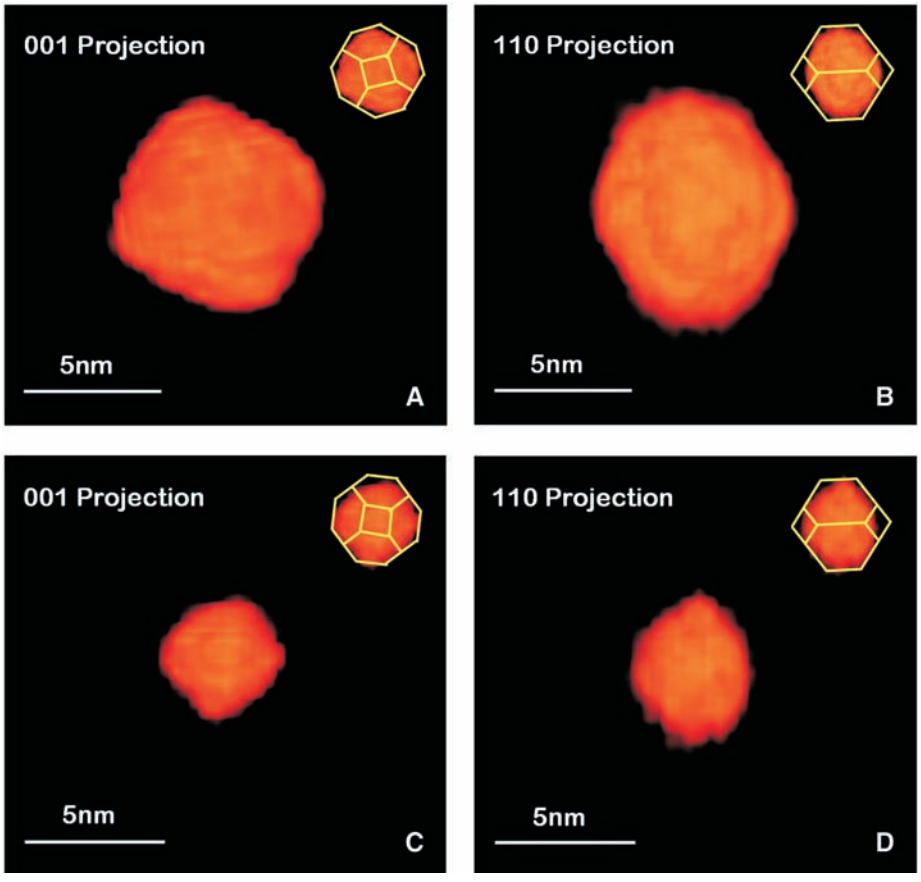

Fig. 2. (**A**) A reconstruction of a 7-nm in-layer quantum dot in plan view, with an inset showing good agreement with the truncated octahedron shape. (**B**) The same dot in cross section, again with good agreement. (**C** and **D**) present the out-of-layer 3.5-nm quantum dot and show that this dot is not uniform, but is formed by filling a void in Si from one side to the other. The quantum dots in this figure are all volume rendered.

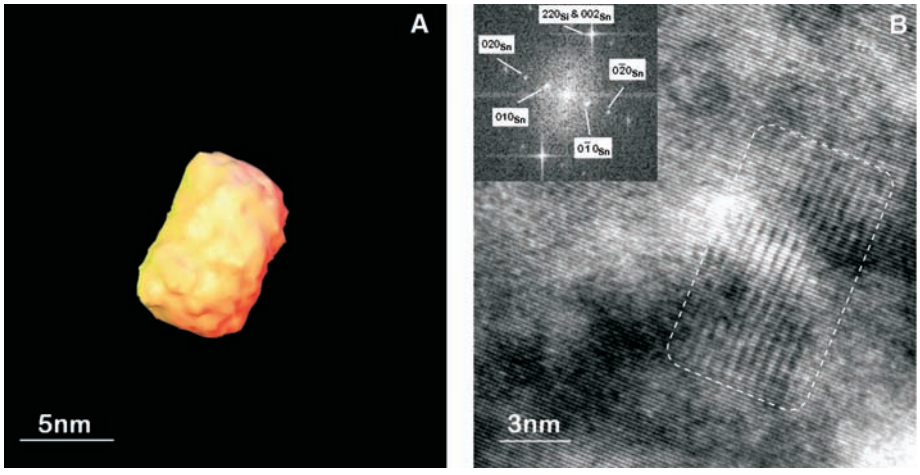

Fig. 3. (**A**) Surface rendered reconstruction of a β-Sn dot showing a clear elongation of the dot. The fine scale surface roughness here is an artifact of the reconstruction process. (**B**) High-resolution TEM image with a fast Fourier transform inset, showing that these β-Sn dots have a different crystal structure than that of α-Sn (the β-Sn dot is outlined in a dashed line). The coherent interface at which growth is fastest is the interface between $(220)_{Si}$ and $(020)_{\beta\text{-}Sn}$.

A number of dots in this volume appear elongated in one direction (Fig. 1, D and E). Figure 3A and movie S4 show a reconstruction of one such dot, which has the appearance of a rectangular parallelepiped rather than an octahedron. The difference in size and shape of these dots implies that a different phase is present (β-Sn is the stable phase at room temperature). The presence of β-Sn was confirmed with conventional high-resolution TEM, and Fig. 3B shows a lattice image of one such dot. The rectangular projection is revealed, and a Fourier transform of the dot (Fig. 3B, inset) confirms that the crystal structure is different from the face-centered cubic α-Sn structure. It appears that beyond a critical diameter of ~8 nm, the α-Sn quantum dots are no longer the energetically favorable structure, and they transform into β-Sn. The 3D reconstructions are the only way to verify the nature of this transformation. From Fig. 3, A and B, it is clear that the transformation leads to an elongation of the Sn dot in one of the in-plane $<110>_{Si}$ directions and in particular, the development of

a favored interface between the β-Sn and the (110) planes in the Si matrix. The excellent lattice match between the (100) planes of the β-Sn and the (110) Si is clearly the driving force for this elongation, leading to an extended coherent interface. Symmetry allows an equivalent elongation in the perpendicular in-plane $<110>_{Si}$ direction (Fig. 1D).

High-resolution Z-contrast tomography in the STEM was used to elucidate the formation mechanism of embedded quantum dots. We have identified embedded quantum dots with both the α-Sn and β-Sn phases, with a transformation into β-Sn beyond a critical diameter of ~8 nm. Some quantum dots are formed outside the embedded layers due to diffusion of Sn from the layers to fill Si voids. These dots are formed by Stranski-Krastonov growth, filling from one side of the void to the other after an initial wetting of the surface of ~1 to 2 monolayers. These results demonstrate that STEM tomography can directly determine the location, size, shape, structure, and formation mechanism of embedded nanostructures in 3D with a resolution of 1 nm^3, which is essential information for all of the nanosciences.

References and Notes

1. X. Michalet *et al.*, *Science* **307**, 538 (2005).
2. Y. Lin *et al.*, *Nature* **434**, 55 (2005).
3. A. P. Alivisatos, *J. Phys. Chem.* **100**, 13266 (1996).
4. T. Mokari, E. Rothenberg, I. Popov, R. Costi, U. Banin, *Science* **304**, 1787 (2004).
5. J. Su *et al.*, *Appl. Phys. Lett.* **86**, 013105 (2005).
6. J. M. Cowley, *Principles and Techniques of Electron Microscopy; Biological Applications* (Van Nostrand Reinhold, New York, 1976), vol. 6.
7. S. B. Chikkannanavar, D. E. Luzzi, S. Paulson, A. T. Jonson Jr., *Nano Lett.* **5**, 151 (2005).
8. N. D. Browning, M. F. Chisholm, S. J. Pennycook, *Nature* **366**, 143 (1993).
9. S. J. Pennycook, L. A. Boatner, *Nature* **336**, 565 (1988).
10. E. M. James, N. D. Browning, *Ultramicroscopy* **78**, 125 (1999).
11. P. E. Batson, N. Dellby, O. L. Krivanek, *Nature* **418**, 617 (2002).
12. I. Arslan, A. Bleloch, E. A. Stach, N. D. Browning, *Phys. Rev. Lett.* **94**, 025504 (2005).
13. P. A. Midgley, M. Weyland, *Ultramicroscopy* **96**, 413 (2003).
14. L. Goldstein, F. Glas, J. Y. Marzin, M. N. Charasse, G. Le Roux, *Appl. Phys. Lett.* **47**, 1099 (1985).
15. D. Leonard, M. Krishnamurthy, C. M. Reaves, S. P. DenBaars, P. M. Petroff, *Appl. Phys. Lett.* **63**, 3203 (1993).
16. T. P. Pearsall, Ed., *Quantum Semiconductor Devices and Technologies*, (Kluwer Academic Publishers, Dordrecht, Netherlands, 2000).
17. R. Ragan, K. S. Min, H. A. Atwater, *Mater. Sci. Eng. B* **87**, 204 (2001).
18. Y. Lei *et al.*, *Appl. Phys. Lett.* **82**, 4262 (2003).
19. P. Mock *et al.*, *Proc. SPIE* **4807**, 71 (2002).
20. V. V. Voronkov, R. Falster, *J. Cryst. Growth* **198-199**, 399 (1999).
21. J. Jinschek, U. Kaiser, W. Richter, *J. Electron Microsc.* **50**, 3 (2001).
22. D. J. Eaglesham, A. E. White, L. C. Feldman, N. Moriya, D. C. Jacobson, *Phys. Rev. Lett.* **70**, 1643 (1993).
23. R. W. Vook, *Int. Metals Rev.* **27**, 209 (1982).
24. A. Zangwill, *Physics at Surfaces*, (Cambridge Univ. Press, Cambridge, 1988), pp. 427–432.
25. D. H. Rich, T. Miller, A. Samsavar, H. F. Lin, T.-C. Chiang, *Phys. Rev. B* **37**, 10221 (1988).
26. A. Charrier *et al.*, *J. Phys. Condens. Matter* **13**, L521 (2001).
27. M. Yoshimura, B. An, K. Yokogawa, K. Ueda, *Appl. Phys. A* **66**, S1047 (1998).

28. This work was supported by the Royal Society and the NSF in the form of fellowships for I.A. We thank J. Barnard, the FEI Company, and P. Moeck for helpful discussions and H. Atwater for the samples. The Engineering and Physical Sciences Research Council, the Cambridge Interdisciplinary Research Collaboration in Nanotechnology, the FEI Company, and the Isaac Newton Trust are thanked for financial assistance. This work was supported in part by the U.S. Department of Energy under grant number DE AC05-03ER46057.

Supporting Online Material

www.sciencemag.org/cgi/content/full/309/5744/2195/DC1
Movies S1 to S4

29 June 2005; accepted 2 September 2005
10.1126/science.1116745

Colloidal Jamming at Interfaces: A Route to Fluid-Bicontinuous Gels

K. Stratford,[1] R. Adhikari,[2] I. Pagonabarraga,[2,3] J.-C. Desplat,[1,4] M. E. Cates[2]*

Colloidal particles or nanoparticles, with equal affinity for two fluids, are known to adsorb irreversibly to the fluid-fluid interface. We present large-scale computer simulations of the demixing of a binary solvent containing such particles. The newly formed interface sequesters the colloidal particles; as the interface coarsens, the particles are forced into close contact by interfacial tension. Coarsening is markedly curtailed, and the jammed colloidal layer seemingly enters a glassy state, creating a multiply connected, solidlike film in three dimensions. The resulting gel contains percolating domains of both fluids, with possible uses as, for example, a microreaction medium.

The search for new materials with mesoscale or nanoscale structure is a major theme of current physical science. Routes that exploit spontaneous self-assembly in thermal equilibrium are important (*1*, *2*), but nonequilibrium processes offer more control—because assembly is then governed not just by thermodynamic conditions but by the entire process history [e.g., (*3*–*5*)]. Moreover, the resulting materials may become trapped in deeply metastable states such as colloidal clusters, glasses, and gels (*3*, *5*–*7*), remaining more robust than an equilibrium phase to subsequent changes in thermodynamic conditions. This is a key consideration in determining the shelf-life and flow behavior of everyday products such as paint, vaccines, and yogurt.

We use computer simulations to explore a kinetic pathway that leads to the creation of amorphous soft-solid materials. In such a material, which we call a bicontinuous interfacially jammed emulsion gel (or Bijel) (*8*), a pair of interpenetrating, bicontinuous fluid domains are frozen into a permanent arrangement by a densely jammed monolayer of colloidal particles at the fluid-fluid interface. Such materials may have distinctive properties, stemming directly from the nonequilibrium, arrested nature of the monolayer: Bijels should be highly tunable in elasticity and pore size through the volume fraction ϕ and radius a of the solid particles. (The radius can be varied from micrometers to nanometers without altering the physics of structure formation by the route reported here.) One possible application, explored below, is as a cross-flow microreaction medium in which two immiscible fluids are continuously brought into intimate contact by pumping them in opposite directions through a static Bijel.

To achieve maximal stability of a particle-laden interface, the colloidal particles should be chosen with nearly equal affinity for the two liquids involved (*9*). This creates similar values for the two fluid-solid interfacial tensions, and thus a fluid-fluid-solid contact angle close to 90° (known as neutral wetting). A spherical particle is then in stable equilibrium, with its equator positioned at the fluid-fluid interface. In practice, this equilibrium is so stable that detachment of such a particle cannot be achieved by thermal motion alone (*9*). For neutral wetting, the fluid-solid interfaces have the same total energy regardless of particle position, but the fluid-fluid interfacial area is reduced, by a disk of radius a, when the particle lies midway across the interface. The detachment energy ε is the interfacial energy of this disk, $\varepsilon = \sigma\pi a^2$, with σ the fluid-fluid interfacial tension. Hence $\varepsilon/k_BT = (a/a_0)^2$, where $a_0^2 = k_BT/\pi\sigma$ (k_B is the Boltzmann constant and T is temperature). For $T = 300$ K and σ typically ~0.01 Nm^{-1} or larger, a_0 is 0.4 nm or less. Thus, $\varepsilon/k_BT \geq 10$ even for a particle of 1 nm radius, and

[1]EPCC, [2]SUPA, School of Physics, University of Edinburgh, James Clerk Maxwell Building, Kings Buildings, Edinburgh EH9 3JZ, UK. [3]Departament de Física Fonamental, Universitat de Barcelona, C. Martí i Franqués 1, 08028 Barcelona, Spain. [4]Irish Centre for High-End Computing, Dublin Institute for Advanced Studies, 5 Merrion Square, Dublin 2, Ireland.

*To whom correspondence should be addressed. E-mail: m.e.cates@ed.ac.uk